 doi:10.20944/preprints202103.0069.v1

Article

Influence of traditional and solar reflective coatings on the heat transfer of building roofs in Mexico

Iván Hernández-Pérez [1,*]

[1] Universidad Juárez Autónoma de Tabasco, División Académica de Ingeniería y Arquitectura (DAIA-UJAT), Carretera Cunduacán-Jalpa de Méndez km. 1, Cunduacán, Tabasco, CP 86690, México.
* Correspondence: ivan.hernandezp@ujat.mx; Tel.: +52-993-259-0202

Abstract: Building roofs are sources of unwanted heat for buildings situated in zones with a warm climate. Thus, reflective coatings have emerged as an alternative to reject a significant fraction of solar energy received by roofs. In this research, the thermal behavior of concrete slab-type roofs with traditional and solar reflective coatings was simulated using a computational tool. Weather data from four cities in Mexico with a warm climate were used as boundary conditions. This tool is an in-house code based on the Finite Volume Method developed by the author to perform building components simulations. The code was validated with experimental data from previous work. A series of comparative simulations were developed, taking a gray roof as a control case. The results showed that for the roof without thermal insulation (single roof), the solar reflective coatings reduced the exterior surface between 11 and 16°C. Consequently, the single roofs' daily heat gain was reduced by a factor ranging between 41 and 54%. On the other hand, for the insulated roof, the reflective coatings reduced the exterior surface temperature between 17 and 21°C. At the same time, the daily heat gain of composite roofs was reduced between 37 and 56%.

Keywords: Solar reflective coatings; Heat transfer; Heat gains; Building roofs

1. Introduction

The buildings sector used 36% of the total final energy around the world and 39% of energy-related CO_2 emissions in 2018 [1]. Because the population is expected to increase by 2.5 billion people in 2050, the energy use in the building sector is set to rise sharply. In warm locations, the energy consumption from air conditioners is high due to the heat flow received by buildings situated in these zones. The building envelope plays a vital role in the thermal interaction between the outdoor and indoor environments. Thus, it is important to minimize the energy gain from the building envelope to avoid the excessive use of electricity for comfort purposes.

Today several technologies are available for building energy retrofitting. There are advanced facades [2], high insulated windows [3], high insulation levels for roofs and walls [4], reflective coatings [5], phase change materials [6], and well-sealed structures [7], to mention a few. Particularly, reflective surfaces are becoming popular for two main reasons. First, because the most direct way to reduce the incident solar energy is to reflect it. When new, solar reflective coatings can reflect to the sky up to 90% of the solar energy received by a surface. The second reason is that applying reflective coatings to opaque building components is probably the most simple passive measure because most of these coatings can be installed in the same way as ordinary paint [8]. These coatings are usually used on building roofs because these components are subject to solar radiation for more hours than other building envelope components [9]. Therefore, when a roof is retrofitted with a reflective coating, it is known as a cool roof.

Several researchers around the world have studied the benefits that cool roofs can bring to buildings in different types of climates using a number of approaches. Several experimental studies are available in the literature. For instance, Pisello and Cotana [10] performed a two-year monitoring campaign to test cool roofs in a residential building located in Italy. The results showed that the cool roof solution reduced the peak temperature of the air in attic by around 5°C. Further, the cool roof provided an overall year-round

 doi:10.20944/preprints202103.0069.v1

energy savings that corresponds to 14 kWh/m^2 per year. In China, Quin et al. [11] used a building cell to test different samples of concrete tiles with different solar reflectance. The author performed a series of experiments and found that the tiles with a reflective coating reached lower interior surface temperatures than the control tile. Moreover, an additional 2–6°C cooler temperatures around the noon time was achieved by installing at the tile's bottom with low-emissivity sheathing. Hernández-Pérez et al. [12] evaluated several building roofs with different coatings using two outdoor test cells located in Cuernavaca, Mexico. They showed that in summer the white roof was 29°C cooler than the black roof and just 1.5°C warmer than the ambient air. Further, the average daily energy gain of the white was 73% smaller than the black roof.

Other studies aiming to investigate the year round energy savings from cool roofs by using building energy simulation tools are available. Algarni [13] studied the influence of solar reflective roofs on the energy consumption of residential buildings of Saudi Arabia. The author used eQuest building simulation software to perform simulations of a building prototype using weather data of 13 major cities of this country. The researcher found that a reflective roof reduced the annual energy consumption required for building cooling by between 110.3 and 181.9 kWh/m^2. The maximum increase in annual energy consumption due to winter heating was only 4.4 kWh/m^2. Piselli et al. [14] assessed the effectiveness of cool roofs with optimal insulation levels in different weather conditions worldwide. The authors coupled a dynamic energy simulation tool with an optimization technique to find the best-combined building roof thermal insulation and solar reflectance and minimize the annual energy consumption. The results showed that a high value of solar reflectance reduces the annual energy consumption for most of the analyzed climate zones. Thus, they concluded that the optimal roof configuration must have high solar reflectance and no/low insulation level. Dominguez-Delgado et al. [15] developed an energy and economic life cycle assessment of cool roofs applied to residential buildings in Southern Spain. The simulations demonstrated that the cool roof decreased the annual energy consumption. The maximum decrease found by the authors was 32%, and it was obtained when a roof with solar reflectance of 0.1 was retrofitted with a reflective coating with a solar reflectance of 0.9. The LCA analysis reported that savings were 18.33 €/m^2 and the payback period was around 3 years.

Some researchers have used validated models to predict the benefits of cool roofs. For instance, Tong et al. [16] studied the thermal behavior of ventilated and non-ventilated roofs during a typical day in Singapore. The authors conducted experiments to validate the concrete roof models. Compared with the roofs with a solar reflectance of 0.1, each 0.1 increase in reflectance reduced the daytime heat gain by 11% on the ventilated roofs and the non-ventilated roofs. The reflective coatings application reduced the daily heat gain 234 and 135 Wh/m^2 in the ventilated and non-ventilated roofs, respectively. Further, they indicated that compared to non-ventilated roofs (both reflective and non-reflective), the individual use of ventilation and 2.5 cm of expanded polystyrene (EPS) reduced heat gain by 42 and 68%, respectively. Zingre et al. [17] developed a model to study heat transfer in roofs. They used a spectral approximation method to solve the unsteady one-dimensional heat conduction equation. Furthermore, the model was validated using experimental data obtained from measurements made in two identical apartments with concrete roofs located in Singapore. Model predictions showed that on a sunny day, the reflective coating reduced the maximum roof temperature, indoor air temperature, and daytime heat gain by 14.1 °C, 2.4 °C, and 0.66 kWh/m^2 (54%), respectively.

As shown in the literature review, reflective or cool roofs have brought a series of benefits to the buildings in which they were installed. Thus, it is essential to understand how a cool roof behaves in a particular area. For this purpose, it is necessary to have tools capable of predicting the thermal behavior of a cool roof before its installation to determine if it is feasible from an energy point of view. This work presents the development of a computational tool for modeling the heat transfer of concrete slab-type roofs with traditional and solar reflective coatings. This tool is then used to estimate the temperature

Preprints (www.preprints.org) | NOT PEER-REVIEWED | Posted: 2 March 2021 doi:10.20944/preprints202103.0069.v1

reductions and, consequently, the ability of reflective roofs to modulate the heat gains by implementing this technology in buildings situated in four different warm climates in Mexico.

2. Physical model

Figure 1 shows the physical model of the roof, which is a concrete slab with traditional or solar reflective coating. Two configurations are considered; (a) single roof with a thickness of 10 cm and (b) insulated roof with a thickness of 13 cm. The insulated roof is made of concrete and polystyrene and a thin plaster layer of concrete protects the polystyrene because it should not be exposed to solar radiation. The polystyrene has a thickness equal to 2.5 cm, and the plaster layer has a thickness of 0.5 cm. The width of the roof (W) has been considered 1 m. Both configurations are studied with traditional and solar reflective coatings. The thickness of the coatings has been considered negligible. The materials of both roof configurations are considered homogeneous. The solar absorptance and thermal emissivity of the roofs are also regarded as constant. Further, it is considered that the side surfaces of the two roof configurations are adiabatic. Finally, it is supposed that solar radiation has a normal incidence on the roof and that this is a gray body that only absorbs the incident solar radiation.

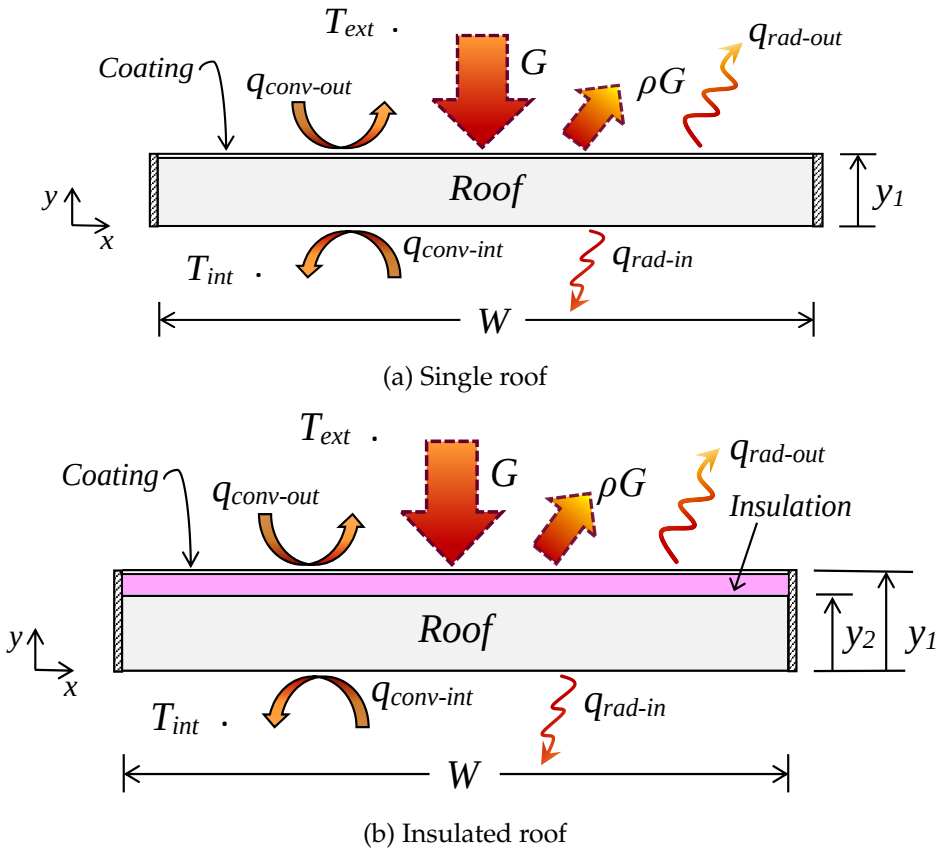

Figure 1. Physical model

3. Mathematical model

The governing differential equation for heat conduction of a two dimensional roof is:

$$\frac{\partial(\rho c_p T)}{\partial t} = \frac{\partial}{\partial x}\left(\lambda \frac{\partial T}{\partial x}\right) + \frac{\partial}{\partial y}\left(\lambda \frac{\partial T}{\partial y}\right) \tag{1}$$

Preprints (www.preprints.org) | NOT PEER-REVIEWED | Posted: 2 March 2021 doi:10.20944/preprints202103.0069.v1

where λ is the thermal conductivity, ρ is the density, and c_p is the specific heat. The boundary conditions used to solve in the physical model are as follows: the exterior surface ($y = y_1$), is in contact with the outdoor environment or environmental conditions of different cities of Mexico. Therefore, the roof has convective and radiative exchange with the surroundings. The lateral surfaces are thermally insulated ($x = 0$ and $x = W$), and the interior surface ($y = 0$) also exchanges heat by convection and radiation with the indoor environment. Mathematically the boundary conditions can be expressed as:

$$-\lambda \frac{\partial T}{\partial y} = \alpha G + h_{out}(T - T_{out}) + \sigma\epsilon(T^4 - T_{sky}^4) \quad \text{for} \quad y = y_1, \quad 0 \leq x \leq W \tag{2}$$

$$-\lambda \frac{\partial T}{\partial y} = h_{in}(T - T_{in}) \quad \text{for} \quad y = 0, \quad 0 \leq x \leq W \tag{3}$$

$$\frac{\partial T}{\partial x} = 0 \quad \text{for} \quad x = 0, \quad 0 < y < y_1 \tag{4}$$

$$\frac{\partial T}{\partial x} = 0 \quad \text{for} \quad x = W, \quad 0 < y < y_1 \tag{5}$$

In eq. (2), G is the solar radiation received by the roof, α is the solar absorptance of the coating, ϵ is the thermal emittance and σ is the Stefan–Boltzmann constant. To calculate the outdoor convective heat transfer coefficient (h_{out}) in eq. (2), the following empirical correlation was used [18]:

$$h_{out} = 2.8 + 3.0v \tag{6}$$

Where v is the wind speed in m/s and h_{out} is the outdoor convective heat transfer coefficient in W/m^{2}K. The value of T_{sky} is calculated with the following expression [18]:

$$T_{sky} = 0.0552 T_{out}^{1.5} \tag{7}$$

In equation (7), T_{out} is the outdoor air temperature, both temperatures T_{sky} y T_{out} are expressed in K. The heat transfer coefficient in the interior environment h_{in} in the equation (3) which considers both convection and thermal radiation is equal to 6.13 W/m^2 when the heat flux heat goes to the indoor air, and 9.26 W/m^{2}K when the heat flux goes from the indoor air to the interior surface [19].

4. Solution methodology for the roof model

This section present the methodology followed to solve numerically the heat conduction equation (1). The following steps were developed:

- Generation of the computational mesh.
- Discretization of the mathematical model.
- Solution of the system of algebraic equations.

The discretization technique used in this work was the finite volume method (FVM), the following subsections describe each of these steps.

4.1. Generation of the computational mesh

This step consists of dividing the domain into small control volumes where the nodes are situated, and the value of the temperature $T(x, y)$ is determined. In this analysis, the main node P is located in the center of the control volume (Figure 2), so that the its interface (point w, e, n and s) is at the middle from one node to another.

The equation (8) describes the distribution of the nodes in the mesh in the direction of x:

Preprints (www.preprints.org) | NOT PEER-REVIEWED | Posted: 2 March 2021 doi:10.20944/preprints202103.0069.v1

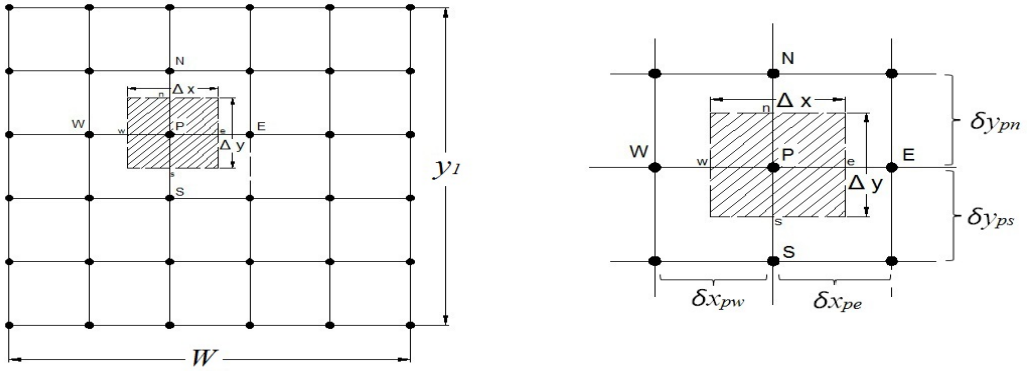

Figure 2. A control volume in the computational mesh

$$x(i) = \frac{W}{N_x - 1}(i-1) \quad \text{for} \quad i = 1, 2, 3, ..., N_x \tag{8}$$

where N_x is the number of nodes in x and direction, and W is the width of the building roof (Figure 1). This equation provides the direction coordinate of the nodes x. For the nodes in direction y its coordinate is given by:

$$y(j) = \frac{y_1}{N_y - 1}(j-1) \quad \text{for} \quad j = 1, 2, 3, ..., N_y \tag{9}$$

where N_y is the number of nodes in y and direction, and y_1 is the height of the building roof (Figure 1). It is also necessary to know the thickness of the control volume in both directions, the equation (10) is used to calculate such thicknesses

$$\Delta x = \frac{W}{N_x - 1} \qquad \Delta y = \frac{y_1}{N_y - 1} \tag{10}$$

4.2. Discretization of the mathematical model

Discretization consists of applying a technique to transform the partial differential equation of the mathematical model to a set of algebraic expressions to facilitate its solution. For the internal nodes, the equation (1) governs their behavior it and can be represented by:

$$\frac{\partial \rho\phi}{\partial t} = \frac{\partial}{\partial x}\left(\Gamma \frac{\partial \phi}{\partial x}\right) + \frac{\partial}{\partial y}\left(\Gamma \frac{\partial \phi}{\partial y}\right) \quad \text{for} \quad 0 < x < W; \quad 0 < y < y_1$$

Where: $\phi = T$, $\Gamma = \lambda / c_p$. Taking the domain of interest, for each term of the previous equation, between the points w and e in the x-direction of the control volume in Figure 2, and between the points n and s in the y- direction; Furthermore, considering the time step, a domain of interest is taken from an earlier time (t_0) to a later time ($t = t_0 + \Delta t$)

$$\int_{t_0}^{t}\int_{s}^{n}\int_{w}^{e} \frac{\partial \rho\phi}{\partial t}\, dx\, dy\, dt = \int_{s}^{n}\int_{w}^{e} \frac{\partial}{\partial x}\left(\Gamma \frac{\partial \phi}{\partial x}\right) dx\, dy + \int_{s}^{n}\int_{w}^{e} \frac{\partial}{\partial y}\left(\Gamma \frac{\partial \phi}{\partial y}\right) dx\, dy + \int_{s}^{n}\int_{w}^{e} S\, dx$$

Integrating in the space the previous equation over the control volume, the following it is obtained

Preprints (www.preprints.org) | NOT PEER-REVIEWED | Posted: 2 March 2021 doi:10.20944/preprints202103.0069.v1

$$\left[\frac{\partial\overline{\rho\phi}}{\partial t}\right]\Delta x\Delta y = \left[\left(\Gamma\frac{\partial\phi}{\partial x}\right)_e - \left(\Gamma\frac{\partial\phi}{\partial x}\right)_w\right]\Delta y + \left[\left(\Gamma\frac{\partial\phi}{\partial y}\right)_n - \left(\Gamma\frac{\partial\phi}{\partial y}\right)_s\right]\Delta x + \overline{S}\Delta x\Delta y$$

Now using an implicit interpolation scheme for time

$$\begin{aligned}\left[\frac{(\rho\phi)_P^t - (\rho\phi)_P^{t_0}}{\Delta t}\right]\Delta x\Delta y &= \left[\left(\Gamma\frac{\partial\phi}{\partial x}\right)_e^t - \left(\Gamma\frac{\partial\phi}{\partial x}\right)_w^t\right]\Delta y + \left[\left(\Gamma\frac{\partial\phi}{\partial y}\right)_n^t - \left(\Gamma\frac{\partial\phi}{\partial y}\right)_s^t\right]\Delta x \\ &+ \overline{S}\Delta x\Delta y\end{aligned}$$

Because the conditions at the interfaces are unknown, the centered scheme interpolation was used, using the known values of the nodes adjacent to that control volume interface (node E, W, N and S), the following is obtained

$$\begin{aligned}\left[\frac{(\rho\phi)_P^t - (\rho\phi)_P^{t_0}}{\Delta t}\right]\Delta x\Delta y &= \Gamma_e\left(\frac{\phi_E - \phi_P}{\delta x_{PE}}\right)\Delta y - \left(\frac{\phi_P - \phi_W}{\delta x_{PW}}\right)\Delta y + \Gamma_n\left(\frac{\phi_N - \phi_P}{\delta y_{PN}}\right)\Delta x \\ &- \Gamma_s\left(\frac{\phi_P - \phi_S}{\delta y_{PS}}\right)\Delta x + \overline{S}\Delta x\Delta y\end{aligned}$$

It is convenient to group the terms of the equation into coefficients as follows

$$\phi_P\underbrace{\left[\left(\frac{\rho\Delta x\Delta y}{\Delta t}\right) + \left(\frac{\Gamma_e}{\delta x_{PE}} + \frac{\Gamma_w}{\delta x_{PW}}\right)\Delta y + \left(\frac{\Gamma_n}{\delta y_{PN}} + \frac{\Gamma_s}{\delta y_{PS}}\right)\Delta x\right]}_{a_P} = \phi_E\underbrace{\left(\frac{\Gamma_e\Delta y}{\delta x_{PE}}\right)}_{a_E}$$

$$+\phi_W\underbrace{\left(\frac{\Gamma_w\Delta y}{\delta x_{PW}}\right)}_{a_W} + \phi_N\underbrace{\left(\frac{\Gamma_n\Delta x}{\delta y_{PN}}\right)}_{a_N} + \phi_S\underbrace{\left(\frac{\Gamma_s\Delta x}{\delta x_{PS}}\right)}_{a_S} + \underbrace{\phi_P^{t_0}\underbrace{\left(\frac{\rho\Delta x\Delta y}{\Delta t}\right)^{t_0}}_{a_P^0} + \overline{S}\Delta x\Delta y}_{b}$$

Therefore

$$a_E = \frac{\Gamma_e\Delta y}{\delta x_{PE}} \qquad a_W = \frac{\Gamma_w\Delta y}{\delta x_{PW}} \qquad a_N = \frac{\Gamma_n\Delta x}{\delta y_{PN}} \qquad a_S = \frac{\Gamma_s\Delta x}{\delta x_{PS}}$$

$$a_P^0 = \frac{\rho\Delta x\Delta y}{\Delta t}$$

$$b = S\Delta x\Delta y + a_P^0\phi_P^0$$

$$a_P = a_E + a_W + a_N + a_S + a_P^0 - \overline{S}\Delta x\Delta y$$

Obtaining here the equation (11), which is the generative equation of the system of algebraic equations in notation of grouped coefficients

$$a_P\phi_P = a_E\phi_E + a_W\phi_W + a_N\phi_N + a_S\phi_S + b \tag{11}$$

Preprints (www.preprints.org) | NOT PEER-REVIEWED | Posted: 2 March 2021 doi:10.20944/preprints202103.0069.v1

It is necessary to discretize the boundary nodes, according to the physical model, there is a third class condition (interior surface of the roof), two second class conditions at the left and right ends and another third class with radiative loss or gain in the exterior surface.

4.3. Solution of the system of algebraic equations.

If the system of algebraic equations resulting from the discretization of a two-dimensional model is adjusted in a matrix way, it is obtained a matrix of pentagonal and diagonally dominant coefficients. For the one-dimensional case, the Thomas algorithm or tridiagonal matrix algorithm (TDMA) is applied as a direct method by the dominant tridiagonal matrix of coefficients; however, Thomas's algorithm can be used for the two-dimensional case by combining it with iterative equation solving methods. In this work, The system of algebraic equations was solved using the line by line Gauss-Seidel method with alternating directions (LGS-ADI).

5. Verification and validation of the numerical code

The numerical code was developed in the Fortran programming language, and it was verified by comparing its results against the analytical solution for a composite solid reported by Chen and Paine [20]. The most significant deviation between the numerical solution and the analytical results were found for the isothermals of 300 and 250 °C. The maximum difference was 3.0%.

To validate the numerical code that solves the heat conduction equation, experimental data from previous publication of the author was used [21]. The numerical code was validated for two cases: a conventional gray roof and a white reflective roof. In the experiment performed by Hernández-Pérez et al. [21] with two test cells the exterior surface temperature of the roofs was measured every 10 min for five days. Figure 3 shows the temperatures obtained by solving the model and the experimental temperatures. This figure shows that the model satisfactorily predicts the behavior of the gray roof and the white reflective roof. The maximum deviations of the temperatures obtained for the gray and white roofs were 5.5% and 4.6%, respectively. Therefore, this model can be used to study the thermal performance of concrete roof slabs in different weather conditions.

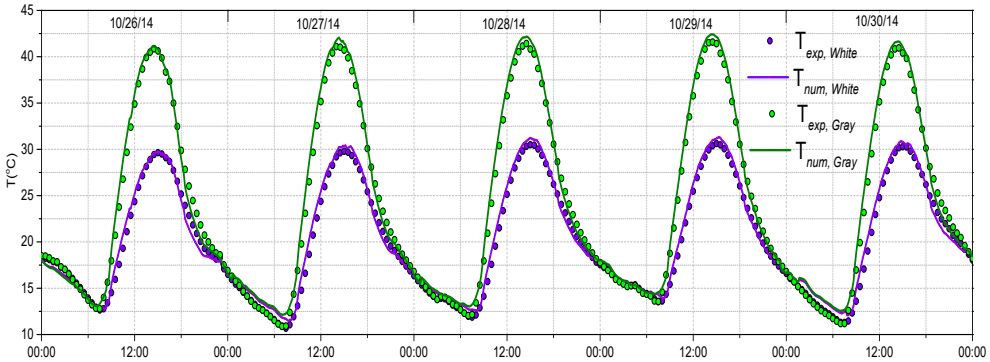

Figure 3. Comparison of experimental data from Hernández-Pérez et al. [21] and data obtained with the numerical model.

6. Weather data

Once the roof model has been verified and validated, its thermal behavior is studied under the outdoor environment of different cities. It was used data from four representative towns in Mexico with warm weather. Table 1 shows the four major cities with their corresponding type of weather. The weather data used for the simulations were filtered from files provided by the National Meteorological Service-National Commission of Water (SMN-CONAGUA), the public body responsible for providing information on the state

Preprints (www.preprints.org) | NOT PEER-REVIEWED | Posted: 2 March 2021 doi:10.20944/preprints202103.0069.v1

of the weather that prevails or affects the territory of this country. The SMN-CONAGUA obtains the weather data files from weather stations situated in each city. The data files contained several recorded variables every ten minutes for a whole year. Still, it was only used solar radiation, wind speed, and air temperature for the simulations, as shown in results section. The thermal behavior of the roofs was analyzed for the week with the highest temperatures of the year 2018.

Table 1: Representative cities of the zones with warm weather in Mexico.

City	Weather type
Hermosillo, Sonora	Warm dry
Monterrey, N.L.	Warm semi-dry
Villahermosa, Tabasco	Warm humid
Mérida, Yucatán	Warm semi-humid

7. Properties of traditional and reflective coatings

Table 2 shows the values of solar reflectance and thermal emittance of the four coatings analyzed in this research. There are two traditional coatings, gray and terracotta, and two solar reflective coatings, white # 1 and white # 2. These optical properties of the coatings were measured in two previous works of the author [12,21].

Table 2: Optical properties of the coatings.

Coating	Solar absorptance (α)	Thermal emittance (ε)
Gray	0.67	0.87
Terracotta	0.70	0.88
White # 1	0.20	0.90
White # 2	0.16	0.89

8. Results

This section presents the concrete roof's behavior with four coatings in terms of the temperature of the exterior surface, the temperature of the interior surface, and the heat flux traveling through the roofs. Further, the cumulative heat gain is obtained by determining the area under the heat flux curve for each day. This section shows first the results for the single roof configuration and then the corresponding for the composite roof configuration.

8.1. Single roof

As mentioned above, the roofs' thermal behavior was analyzed using the weather data of the week with the warmest outdoor air temperatures of 2018 using weather data from four representative towns in Mexico with warm climate. The detailed results of Hermosillo are shown here because it is the town with the highest outdoor temperature. At the end of this subsection a summary table presents the results of the thermal evaluation of the single roof in all cities.

For Hermosillo Sonora, the days selected were from May 30 to June 5, 2018 because it was the week with the highest temperatures of the year. Figure 4(a) shows the solar irradiation and the wind speed during the seven days analyzed. The maximum solar radiation is around 1000 W/m^2. According to the behavior of solar irradiance, all days selected are clear days without clouds. The maximum wind speed reached around 5 m/s. Figure 4(b) shows the air temperature; due to the type of weather of this city, the ambient air reaches very high temperatures, with an average maximum temperature of 45°C.

Figure 4(b) presents the temperature of the exterior surface of the roofs and the ambient air temperature during the selected week. Conventional roofs have similar behavior, and,

Preprints (www.preprints.org) | NOT PEER-REVIEWED | Posted: 2 March 2021 doi:10.20944/preprints202103.0069.v1

on the other hand, reflective roofs maintain a similar behavior concerning the temperature of the exterior surface. This effect occurs because the solar reflectance of conventional coatings is very similar. The exterior surface of the roofs reached its maximum temperature between 14:30 and 15:00 hrs. The exterior surface of the single terracotta roof (STR), the single gray roof (SGR), the single white roof #1 (SWR1), and the single white roof #2 (SWR2) reached on average 61, 59, 45, and 43°C, respectively. These values indicate that applying the terracotta coating, on average, increases the temperature of the exterior surface by 2°C compared to the SGR. In contrast, SWR1 and SWR2 reduced the temperature of the exterior surface average 14 and 16°C, respectively. Furthermore, if the average maximum temperatures of reflective roofs are compared with the average maximum temperature of ambient air (45°C), it is obtained that the SWR1 had the same maximum temperature as ambient air. In contrast, the SWR2 reached a temperature of 2°C lower than the maximum air temperature. On the other hand, the SGR and STR reached a temperature of 14 and 16°C higher than the ambient air temperature.

Figure 4(c) presents the temperature of the single roofs' interior surface. The interior surface of the roofs reached their maximum temperature between 16:00 and 16:40 hrs. The temperature of the interior surface of the STR, SGR, SWR1, and SWR2 reached a maximum temperature of 51, 49, 38, and 37°C, respectively. Therefore, the influence of a reflective coating on the interior surface temperature is obtained by comparing the previous temperature values. The SWR1 decreased the temperature of the interior surface by around 10°C compared to an SGR, while an SWR2 reduced the temperature of this surface by around 11°C.

Figure 4 (d) shows the behavior of the heat flux of the roofs in Hermosillo during the seven days analyzed. The maximum heat flux traveling through the roofs occurs between 16:00 and 16:50 hrs. STR, SGR, SWR1, and SWR2 had an average peak heat flux of 157, 150, 87, and 82 W/m^2, respectively. These values indicate that the peak heat flux crossing the SWR1 and SWR2 is 41% and 45% smaller than the corresponding to the SGR. While the heat flux of the STR is 5% greater than the one of the SGR. The cumulative heat gain for one day or daily heat gain is obtained by calculating the area under the heat flux curve for each day. During the seven days analyzed, the STR had an average heat gain of 1,793 W·h/(m^2-day), the SGR a gain of 1,675 W·h/(m^2-day), the SWR1 of 1,045 W·h/(m^2-day) and the SWR2 roof 993 W·h/(m^2-day). Thus, by calculating the percentage difference between the average daily heat gain, it was found that a TSR located in Hermosillo had a 7% greater heat gain than an SGR, while SWR1 and SWR2 roofs have 38 and 41% less heat gain than a gray roof.

A similar procedure for the other three cities was developed to perform the simulations; it was selected the week with the warmest outdoor air temperatures of 2018. The weather data from this week was introduced to the simulation tool. Table 3 presents a summary of the results obtained from the evaluation of the single roof with traditional and solar reflective coatings in the four cities of Mexico. The table shows the average peak surface temperatures (T_{es} and T_{is}), the average peak heat flux (Q_R), and the average daily heat gain of the roofs (HG). Taking the SGR as a reference, the percentage differences between the peak heat flux of this roof and the other cases were also determined within parenthesis (%) in the table, and the same was done for the heat gain. Table 3 demonstrates that the SWR1 and SWR2 were able to reduce T_{es} between 11 and 16°C compared to the gray roof. Thus, the peak heat flux crossing the SGR can be shaved between 42 and 57% due to a white reflective coating application. Further, SWR1 and SGR2 reduced HG between 41 and 85%. On the other hand, the STR reached a maximum temperature 2°C above the SGR temperature in all cities. These higher temperatures caused an increase in the daily heat gain between 7 and 11%

Preprints (www.preprints.org) | NOT PEER-REVIEWED | Posted: 2 March 2021 doi:10.20944/preprints202103.0069.v1

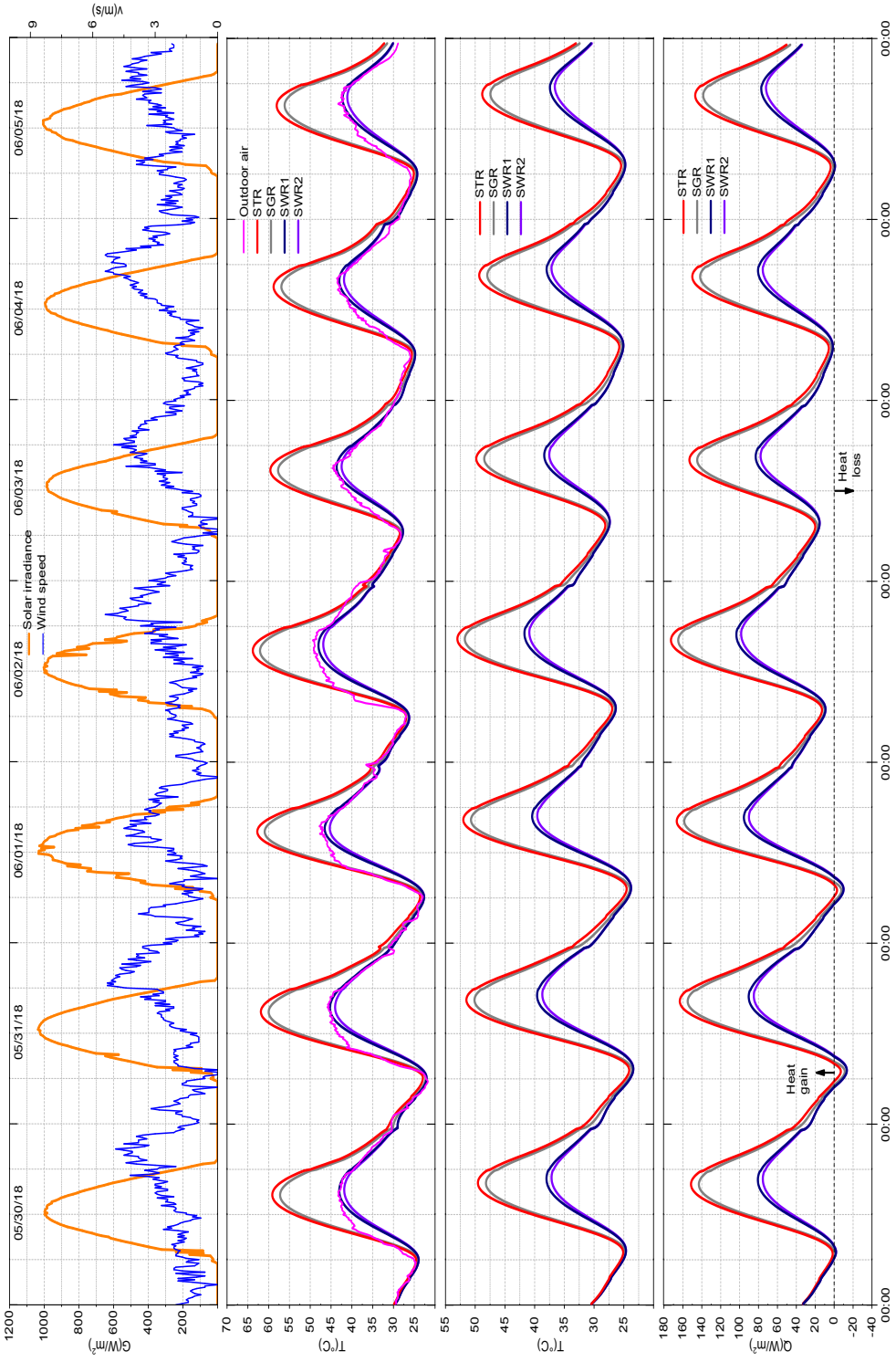

(a) Solar irradiance and wind speed

(b) Temperature of exterior surface and outdoor air

(c) Temperature of interior surface

(d) Heat flux of the roofs

Figure 4. Thermal behavior of the single roof with traditional and solar reflective coatings in Hermosillo

Preprints (www.preprints.org) | NOT PEER-REVIEWED | Posted: 2 March 2021 doi:10.20944/preprints202103.0069.v1

Table 3: Summary of the thermal evaluation of single roof in four cities of Mexico (Average peak values for the different variables).

City	Roof	T_{es} (°C)	T_{is} (°C)	Q_R ($\frac{W}{m^2}$)	HG ($\frac{W \cdot h}{m^2 - day}$)
Monterrey	SGR	51	43	113	1,109
	SWR1	38	34	56 (-50%)	563 (-49%)
	SWR2	37	33	52 (-54%)	520 (-53%)
	STR	53	45	121 (+7%)	1,213 (+9%)
Hermosillo	SGR	59	49	150	1,675
	SWR1	45	39	87 (-42%)	1,045 (-38%)
	SWR2	43	38	82 (-45%)	993 (-41%)
	STR	61	51	157 (+5%)	1,793 (+7%)
Villahermosa	SGR	50	43	111	1,097
	SWR1	37	34	53 (-52%)	550 (-50%)
	SWR2	36	33	48 (-57%)	506 (-54%)
	STR	52	44	120 (+8%)	1,219 (+11%)
Mérida	SGR	53	43	123	1,148
	SWR1	39	34	61 (-50%)	569 (-50%)
	SWR2	38	33	56 (-54%)	511 (-54%)
	STR	55	44	131 (+7%)	1255 (+9%)

8.2. Insulated roof

The insulated roof was studied also in Hermosillo for being warmest city among the selected locations. As in the previous section, first the detailed analysis of this city is presented and then the results for other cities are summarized at the end of this subsection.

Figure 5(b) shows the behavior of the temperature of the external surface of the insulated roofs and the temperature of the ambient air during the seven days considered. Insulated roofs with a conventional color have a similar behavior, and on the other hand, the insulated roofs with reflective coating maintain a similar behavior regarding the temperature of the exterior surface. The exterior surface of the roofs reached its maximum temperature between 13:30 and 14:00 hrs. The exterior surface of the insulated terracotta roof (ITR) reached on average 72°C, the insulated gray roof (IGR) 69°, the insulated white roof #1 (IWR1) 50°C, and the insulated white roof #2 (IWR2) 49°C. These temperatures indicate that ITR had on average a temperature of the exterior surface about 3°C higher than the IGR. While IWR1 and IWR2 reduced the temperature of the exterior surface by an average of 19 and 20°C, respectively. If the average maximum temperatures of white reflective roofs are compared with the average maximum temperature of ambient air (45°C), it is obtained that the IWR1 had a maximum temperature of 5°C above the maximum air temperature, while the IWR2 roof reached a temperature 4°C higher than the maximum air temperature. On the other hand, the IGR and ITR reached a temperature of 23 and 26°C higher than the maximum ambient air temperature, respectively.

Figure 5(c) shows the temperature of the interior surface of the four roofs. Due to thermal insulation, the temperatures of the roofs' interior surface have a small oscillation between day and night compared to the cases without insulation. This surface reached their maximum temperature between 17:30 and 18:10 hrs. The temperature of the interior surface of the ITR and that of the IGR reached a maximum temperature of 29.3°C and 29°C, while the surface temperature of the IWR1 and the IWR2 reached 27.4°C and 27.2°C. This figure demonstrates that the insulation causes the interior temperature of the roofs to remain relatively constant.

Figure 5(d) shows the behavior of the heat flux of the insulated roofs in Hermosillo.

Preprints (www.preprints.org) | NOT PEER-REVIEWED | Posted: 2 March 2021 doi:10.20944/preprints202103.0069.v1

The maximum heat flux traveling through the roofs occurred between 17:30 and 18:10 hrs. Insulated traditional roofs (ITR and IGR) had an average peak heat flux of 27 and 25.3 W/m^2, while insulated white reflective roofs, IWR1 and IWR2, had a peak heat flux of 15.4 and 14.6 W/m^2. As mentioned above, the total heat gain of the roof over a day was determined by calculating the area under the heat flux curve of each day. The composite terracotta roof had an average heat gain of 1,112 J/m^2-day, the gray roof 1,063 J/m^2-day, the white1 669 J/m^2-day, and the white1 roof 635 J/m2-day. The ITR located in Hermosillo had a 6% higher heat gain than the IGR, while IWR1 and IWR2 had a 37 and 40% lower heat gain than the IGR.

Finally, the insulated roofs' thermal behavior was simulated for the remaining cities following the same procedure used for Hermosillo. Table 4 presents a summary of the results obtained from the evaluation of the insulated roofs in the four cities of Mexico. The table shows the values for the average peat temperature of the exterior (T_{se}) and the interior surface (T_{si}), the average peak heat flux of the roofs (Q_R), and the average daily heat gain (HG). Taking the IGR as the control case, the differences between the peak temperatures (T_{se} and T_{si}) were calculated, the peak heat flux (Q_R) and the heat gain (GC). The white reflective roofs were able to reduce T_{se} between 17 and 21°C compared to the IGR. Therefore, they could reduce Q_R that crosses the roofs by a factor ranging between 39 and 54%. Further, these roofs had a HG between 37 and 56% smaller than the ISG. On the other hand, the ITR reached a maximum temperature of 3 °C above the IGR. This temperature increment caused an increase of the Q_R between 7% and 15%. Moreover, the ITR increased the HG by about 11 and 33%.

Another significant result is to analyze the influence of thermal insulation on the roofs' thermal performance. This effect can be obtained from comparing the results presented in Tables 3 and 4. Because the thermal insulation caused the roofs to have indoor surface temperature with small oscillations, the heat flux crossing the insulated roof is very small compared to the one of the single roofs. Thus, the HG of the insulated roofs is four times smaller than the corresponding to the single roofs regardless of the coating and the city. For instance, using the results for Hermosillo, by comparing the HG of the SGR with the HG of the IGR, it can be noticed that the first value is 3.8 smaller than the second value. Therefore, thermal insulation has an essential contribution in reducing heat gains. However, the installation of thermal insulation could more complex and more expensive than applying a reflective coating.

9. Conclusions

It was used a computational tool to simulate the thermal behavior of insulated and non-insulated concrete slab roofs with traditional and solar reflective coatings in four cities with warm climates in Mexico. This simulation tool is a computer code based on the finite volume method that numerically solves the heat conduction equation in unsteady state. The simulations were done using the weather data for the week with the highest outdoor air temperature. Two traditional and two solar reflective coatings installed on the exterior surface of the roofs were considered, and the following is concluded:

Regarding the simulation of the single roofs, the SWR2 was the best configuration to minimize the heat transfer. Due to the small solar absorptance of the coating, the SWR2 presented peak exterior surface temperature up to 16°C lower than the temperature of the SGR. Further, The peak interior surface temperature of the SWR2 was up to 11°C lower than the SGR. Thus, the SWR2 diminished the heat flux, and the daily heat gains up to 57% and 54%, respectively. On the other hand, the simulation indicated that although the exterior surface of the STR was only up to 2°C warmer than the SGR, this temperature increment caused the STR to have a daily heat gain up to 11% greater than the SGR.

The insulated roofs simulations indicated that the surface temperature reduction of the exterior surface due to the reflective coatings was more significant than the single roofs. The IWR2 was the configuration with the best thermal performance. The maximum temperature reduction provided by the IWR2 was 19°C lower than the temperature of the

Preprints (www.preprints.org) | NOT PEER-REVIEWED | Posted: 2 March 2021 doi:10.20944/preprints202103.0069.v1

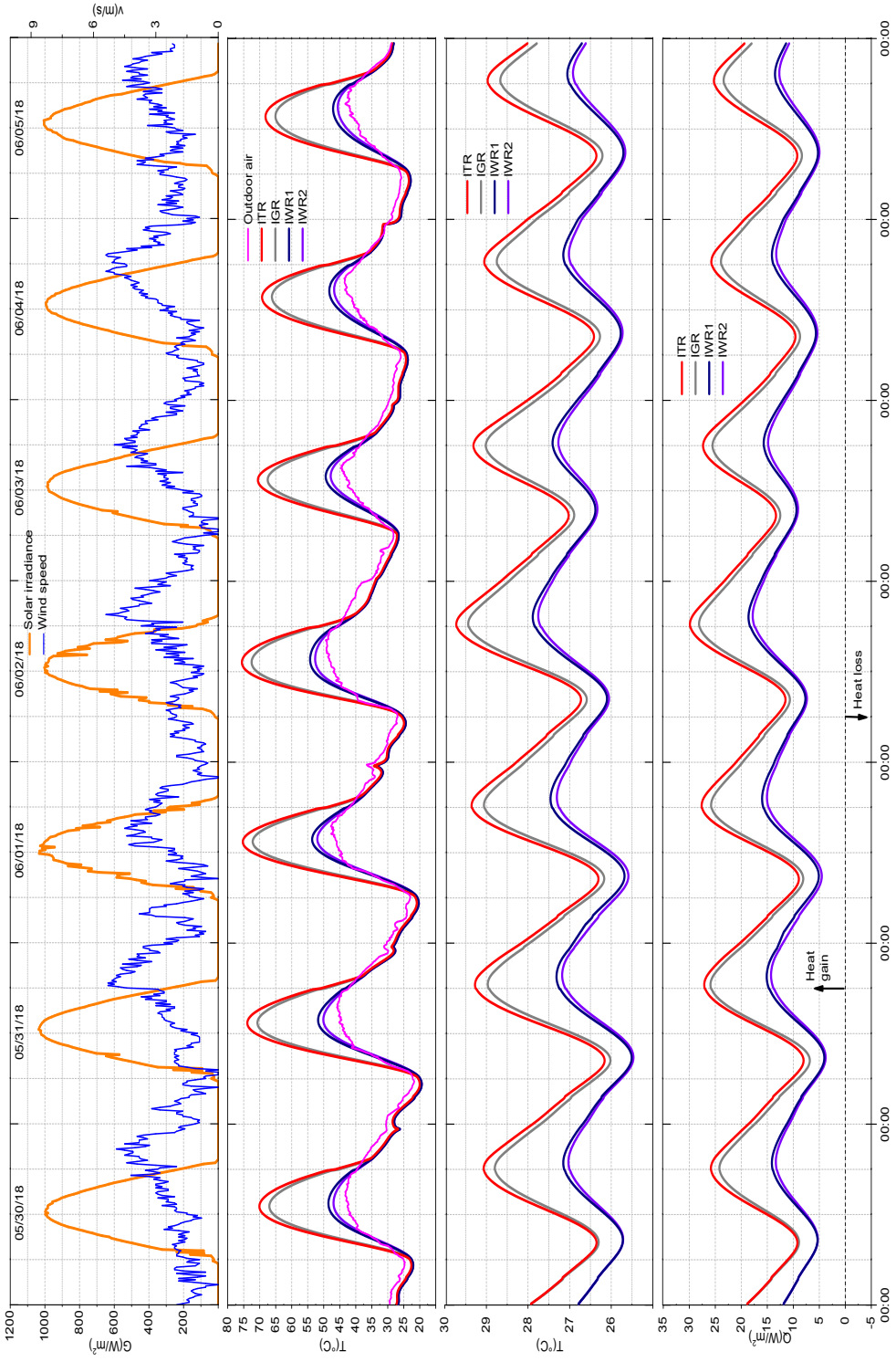

(a) Solar irradiance and wind speed

(b) Temperature of the exterior surface and outdoor air

(c) Temperature of the interior surface

(d) Heat flux of the roofs

Figure 5. Thermal behavior of the insulated roof with traditional and reflective coatings in Hermosillo

Preprints (www.preprints.org) | NOT PEER-REVIEWED | Posted: 2 March 2021 doi:10.20944/preprints202103.0069.v1

Table 4: Summary of the thermal evaluation of insulated roof in four cities of Mexico (Average peak values for the different variables).

City	Roof	T_{es} (°C)	T_{is} (°C)	Q_R ($\frac{W}{m^2}$)	HG ($\frac{W \cdot h}{m^2 - day}$)
Monterrey	IGR	60	27.7	17.1	260
	IWR1	43	26.3	9 (-47%)	128 (-51%)
	IWR2	42	26.2	8 (-53%)	117 (-55%)
	ITR	63	28	19 (+12%)	291 (+12%)
Hermosillo	IGR	69	29	25	439
	IWR1	50	27.4	15.4 (-39%)	276(-37%)
	IWR2	49	27.2	14.6 (-42%)	262 (-40%)
	ITR	72	29.3	27 (+7%)	459 (+6%)
Villahermosa	IGR	58	27.7	13	273
	IWR1	41	26.3	7 (-46%)	140 (-49%)
	IWR2	40	26.1	6 (-54%)	128 (-53%)
	ITR	61	28	15 (+15%)	304 (+11%)
Mérida	IGR	63	27.9	19	284
	IWR1	44	26.4	10 (-47%)	139 (-51%)
	IWR2	42	26.2	9 (-53%)	126 (-56%)
	ITR	66	28.2	21 (+11%)	318 (+12%)

IGR. The IWR2 provided a maximum interior surface temperature reduction 1.6°C, which is very small. This effect occurred because the thermal insulation maintained the interior surface with small oscillations. The IWR2 reduced the peak heat flux and the daily heat gain up to 54% and 15%, respectively.

Finally, because most buildings in Mexico have bare gray or terracotta roofs, there is a great potential for using reflective coatings as a passive measure in this country. This research has demonstrated that white reflective coatings are an excellent alternative to improve the thermal performance of roofs, leading to energy savings and mitigating greenhouse gas emissions.

Funding: "This research received no external funding"

Acknowledgments: The author acknowledges to the National Council of Science of Technology (Conacyt-México) the support provided through the National System of Researchers program (SNI). I am grateful to the Servicio Meteorológico Nacional-Comisión Nacional del Agua (SMN-CONAGUA) for providing the weather data used for the simulations. Finally, the author also acknowledges Jesús Xamán from TecNM-Cenidet for the Finite Volume Method course given to the author.

Conflicts of Interest: "The author declare no conflict of interest."

Abbreviations

The following abbreviations are used in this manuscript:

IGR	Insulated gray roof
ITR	Insulated terracotta roof
IWR1	Insulated white roof #1
IWR2	Insulated white roof #2
SGR	Single gray roof
STR	Single terracotta roof
SWR1	Single white roof #1
SWR2	Single white roof #2

References

1. International Energy Agency (IEA). 2019 Global status report for buildings and construction. Global alliance for building and construction **2019**.
2. Rajcic V., Perkovic N., Bedon C., Barbalic J., Zarnic R. Thermal and energy-efficiency assessment of hybrid CLT–glass facade elements. *Appl Sciences* **2020**, *10*(9), 3071.
3. Wang Z., Tian Q., Jia J. Numerical study on performance optimization of an energy-saving insulated window. *Sustainability* **2021**, *13*(2), 935.
4. Gullbrekken L., Grynning S., Gaarder J.E.Thermal performance of insulated constructions—experimental studies. *Buildings* **2019**, *9*(2), 49.
5. Saber H.H., Hajiah A.E., Alshehri S.A., Hussain H.J. Investigating the effect of dust accumulation on the solar reflectivity of coatings materials for cool roofs applications. *Energies* **2021**, *14*(2), 445.
6. Triano-Juárez J., Macias-Melo E.V., Hernández-Pérez I., Aguilar-Castro K.M., Xamán J. Thermal behavior of a phase change material in a building roof with and without reflective coating in a warm humid zone. *J Build Engineering* **2020**, *32*, 101648.
7. Miszczuk A., Heim D. Parametric study of air infiltration in residential buildings - the effect of local conditions on energy demand. *Energies* **2021**, *14*(1), 127.
8. Hernández-Pérez I., Álvarez G., Xamán J., Zavala-Guillén I., Arce J., Simá E. Thermal performance of reflective materials applied to exterior building components. *Energy Build* **2014**, *80*, 81-105.
9. Todeschi V., Mutani G., Baima L., Nigra M., Robiglio M. Smart solutions for sustainable cities—the re-coding experience for harnessing the potential of urban rooftops. *Appl Sciences* **2020**, *10*(20), 7112.
10. Pisello A.L., Cotana F. The thermal effect of an innovative cool roof on residential buildings in Italy: Results from two years of continuous monitoring *Energy Buildings* **2014**, *69*, 154-164.
11. Qin Y., He Y.0, Wu B., Ma Z. ,Zhang X. Regulating top albedo and bottom emissivity of concrete roof tiles for reducing building heat gains. *Energy Buildings* **2017**, *156*, 218–224.
12. Hernández-Pérez I., Zavala-Guillén I., Xamán J., J.M. Belman-Flores, E.V. Macias-Melo, K.M. Aguilar-Castro. Test box experiment to assess the impact of waterproofing materials on the energy gain of building roofs in Mexico, *Energy* **2019**, *158*, 115847.
13. Algarni S. Potential for cooling load reduction in residential buildings using cool roofs in the harsh climate of Saudi Arabia. *Energy & Environ* **2008**, *30*, 235–253
14. Piselli C., Pisello A.L., Saffari M., de Gracia A., Cotana F., Cabeza L.F. Cool roof impact on building energy need: the roleof thermal insulation with varying climate conditions, *Energies* **2019** *12*, 3354.
15. Dominguez-Delgado A., Dominguez-Torres H., Dominguez-Torres C.A. Energy and economic life cycle assessment of cool roofs applied to the refurbishment of social housing in southern Spain. *Sustainability* **2020**, 12, 5602.
16. Tong S., Li H., Zingre K.T., Wan M.P., Chang V.W.C., Wong S.K., Toh W.B.T. et al.Thermal performance of concrete-based roofs in tropical climate. *Energy Buildings* **2014**, *78* 392-401.
17. Zingre K.T., Wan M.P., Tong S., Li H., Chang V.W.C., Wong S.K., Toh W.B.T., Lee I.Y.L. Modeling of cool roof heat transfer in tropical climate. *Renew Energy* **2016**, *75*, 210–223.
18. Duffie J.A., Beckman W.A., Solar engineering of thermal processes. John Wiley and Sons 1980.
19. Han J., Lin L., Yang H. Investigation on the thermal performance of different lightweight roofing structures and its effect on space cooling load, *Applied Thermal Eng* **2009** *29*, 2491-2499.
20. Chen K.C., Payne U.J., Analytical solution for heat conduction in a two-material-layer slab with linearly temperature Dependent Conductivity, *J. Heat Transfer* **1993**, *113*, 237–239.
21. Hernández-Pérez I., Xamán J., E.V. Macias-Melo, K.M. Aguilar-Castro, Zavala-Guillén I., Hernández-López I., Simá E. Experimental thermal evaluation of building roofs with conventional and reflective coatings, *Energy Build* **2018**, *158*, 569–579.

 doi:10.20944/preprints202103.0069.v1